The old and new Concepts of Physics
An open-dialogue journal
www.uni.lodz.pl/concepts

IMPROVING QUANTUM MICROSCOPY VIA RAMAN PHOTON PAIRS[1]

Marlan O. Scully
Depts. of Chemistry and Mechanical and Aerospace Engineering
Princeton University, Princeton, N.J. 08544-1009
Depts. of Physics and Chemical and Electrical Engineering
Texas A&M University, College Station, TX 77843-4242
Max-Planck-Institut für Quantenoptik
Hans-Kopfermann-Strasse 1, D-85748, Garching, Germany

(Received 20 Apr 2005)

Abstract

In ordinary (classical) microscopy and lithography, the limit of resolution is governed by the wavelength of light used to illuminate the sample. However, by using the correlated photon pairs produced in Raman quantum erasure, the resolution of two-photon quantum microscopy is substantially improved. To that end, we here derive the two-photon quantum state generated by sequential Raman emissions and investigate potential applications. The photon-photon correlation function for Raman pairs is of interest in itself and has features in common with photon antibunching.

[1]Asim Barut enjoyed and brought joy to all of Physics. He was interested in

Photon correlation interferometry [1] is a powerful tool with applications ranging from the macro- to the micro-cosmos. For example, it is well-known that it is possible to improve our ability to measure stellar diameters and resolve binary stars via the Hanbury Brown-Twiss effect.

It is also known that it is possible to improve the resolution of optical microscopy [2] and lithography [3] by using photon correlation interferometry [4]. This has been demonstrated in the elegant experiment of D'Angelo, Chekhova and Shih [5] via two photon down conversion.

We here apply the geometry and physics of the original [2] Raman quantum erasure [6] scheme to resolve molecular markers separated by distances smaller than the wavelength of the probing radiation. As a case in point we note that in many biophysical studies, the shape or conformation of a protein or a DNA strand is monitored as a function of various parameters. One way of making such measurements involves attaching markers, such as dye molecules or quantum dots, to two known points on the protein and observing their fluorescence as they move apart. We here propose and analyze a new, photon-correlation approach, see Fig. 1, to measure the distance between the markers.

Classically, laser light scattered from the two molecules of Fig. 1 generates a "Young's" interference pattern; at detector D1 it is given by $\cos^2\left(k(r_1 - r_1')/2\right) = \cos^2\left(k(d\sin\theta)/2\right)$. The first interference minimum will occur when $kd\sin\theta_m = \pi$. Here d is the distance between the marker molecules, θ_m is the angle between the normal to the line joining the two molecules and the vector pointing to the interference minimum and $k = 2\pi/\lambda$ as usual. Hence, $\lambda/2d = \sin\theta_m < 1$, so that the distance d must be larger than $\lambda/2$ in order to produce the interference pattern. Thus if we wish to measure typical protein features in the 25nm range, we require $\lambda \approx 50$nm.

However, in second order interferometry based on Raman photon pairs the distance d can be measured by shining UV or even visible light on the marker molecules; *i.e.* in the present scheme

literally everything. The present paper uses photon correlation interferometry in a quantum erasure mode to improve resolution. We think Asim would have been interested in this scheme and we dedicate this paper to Asim, our friend and teacher.

$d_{\min} \sim \lambda/13$, see Table 1.

A major portion of the physics behind this enhanced resolution is understood by considering the original Raman quantum eraser configuration of Fig. 1a. Suppose that the molecule is excited by a pulse having frequency $\nu_{\rm p}$ and much later by a pulse at frequency $\nu_{\rm d}$. Then the spontaneous Stokes and anti-Stokes photons of Fig. 1a will be independent, and the Glauber photon-photon correlation function factorizes. To see this we recall

$$G^{(2)}_{\nu,\omega} = \langle\Psi|\hat{E}^{(-)}(1)\hat{E}^{(-)}(2)\hat{E}^{(+)}(2)\hat{E}^{(+)}(1)|\Psi\rangle, \qquad (1)$$

where $G^{(2)}_{\nu,\omega} = G^{(2)}_{\nu,\omega}(1,1';2,2')$, $\hat{E}^{(+)}(1)$ is the positive frequency (an-

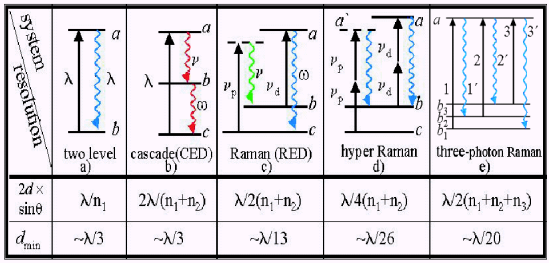

Table 1: Various kinds of marker molecules, for the parameters of Fig. 1, and the associated resolutions are tabulated. In every case λ is the wavelength of the incident light, $\sin\theta = 0.83$ and the refractive indices are $n_1 = 1.9$ while $n_2 = n_3 = 2.1$. (a) Two level scheme yields classical, one photon, resolution. (b) Cascade emission doublet (CED) configuration yields essentially the same resolution as (a). (c) The present Raman erasure doublet (RED) scheme as discussed in the text. (d) Hyper (two-photon) Raman in which $\nu_p \approx \nu_d \approx 2\pi c/\lambda$; the level spacing is not the same scale as in the rest of the Table. (e) Three photon Raman scheme requires correlation between three detectors..

nihilation) part of the electric field and $E^{(-)}(1)$ is the corresponding negative frequency (creation) part; 1 and $1'$ stand for $\mathbf{r}_1, t_1$ and $\mathbf{r'}_1, t'_1$, etc. as in Fig. 1a. The times t_i are controlled by *e.g.*, shutters. The

frequency of the first (Stokes) photon is $\nu = \nu_p + \nu_d - \omega_{ac}$ and the second (antiStokes) is $\omega = \omega_{ac}$.

Now, if the two emitted photons are well separated in time, then the two-photon state $|\Psi\rangle$ can be factorized as a sum of products of one photon Stokes ($|\nu\rangle$) and anti-Stokes ($|\omega\rangle$) states from molecules at A and B, that is

$$|\Psi\rangle = \frac{1}{\sqrt{2}}[|\nu\rangle_A|\omega\rangle_A + |\nu\rangle_B|\omega\rangle_B]. \tag{2}$$

Furthermore, we take advantage of the fact that the first and second photons have different frequencies (ν and ω) and can therefore be separated by, for example, a dichroic mirror. Thus, we can arrange that the ν and ω photons go to, say, detectors 1 and 2 respectively. Equation (1) can then be written as $G^{(2)}_{\nu,\omega} = |\mathcal{E}_{\omega A}(2)\mathcal{E}_{\nu A}(1) + \mathcal{E}_{\omega B}(2)\mathcal{E}_{\nu B}(1)|^2$ using $\mathcal{E}_{\eta A}(i) = \langle 0|\hat{E}^{(+)}(i)|\eta\rangle_A \propto \mathrm{e}^{-i\eta\tau_i}$ and $\mathcal{E}_{\eta B}(i) = \langle 0|\hat{E}^{(+)}(i)|\eta\rangle_B \propto \mathrm{e}^{-i\eta\tau'_i}$ where $\tau_i = t_i - n_i r_i/c$ are the retarded times, r_i (r'_i) are the distances between molecule A (B) and the i^{th} detectors and n_i are the refractive indices with $\eta = \nu$, ω and $i = 1, 2$. It follows that

$$G^{(2)}_{\nu,\omega} = C\cos^2[\frac{1}{2}(\kappa_\nu + \kappa_\omega)d\sin\theta], \tag{3}$$

where $\kappa_\nu = n_1\nu/c$, $\kappa_\omega = n_2\omega/c$ and we have used $r'_1 - r_1 = r'_2 - r_2 = d\sin\theta$. Please note that the detection times $t'_1 = t_1$ and $t'_2 = t_2$. Hence, the interference pattern observed by moving detector 1 (and requiring a correlation with detector 2) is now governed by $k_\nu + k_\omega \simeq 2k$, *i.e.*, the effective radiation wavelength is now $\lambda/2$.

The recent beautiful experiments of Kimble and coworkers [7] and Lukin and coworkers [8] have demonstrated strong correlations between photon pairs generated in the Raman-EIT [9] configuration of Fig. 1a. We find several interesting aspects of the Raman emission doublet (RED) correlation which are qualitatively different from those of a cascade emission doublet (CED) correlation as seen from Fig. 2. We show that microscopic resolution can be significantly enhanced by taking advantage of the RED oscillations of Fig. 2.

In order to develop the properties of the Raman pair state, we consider the case in which the molecules start in level $|c\rangle$, and the $\mathbf{k}$, $\mathbf{q}$ fields are in the vacuum state at time $t = 0$. The Raman pump field of Fig. 1a is assumed to be weak enough and the $b \to a$ laser strong

enough that when the atom is excited to level $|b\rangle$ via the emission of a $\mathbf{k}$ photon, it quickly makes a transition to level a with the emission of a $\mathbf{q}$ photon; and then remains in the ground state for a long time so that it makes sense to seek the state of the field at time $t \to \infty$. After a somewhat lengthy calculation [10], we find the two-photon state as given in Fig. 2. The photon-photon correlation function for a single RED molecule $G^{(2)}(1,2) = |\Psi(1,2)|^2$ is readily calculated from the two photon amplitude $\Psi(1,2) = \langle 0|\hat{E}^{(+)}(2)\hat{E}^{(+)}(1)|\Psi\rangle \equiv \psi(1,2) + \psi(2,1)$ using the RED state $|\Psi\rangle$ of Fig. 2, where

$$\frac{\psi(1,2)}{i\sqrt{\mathcal{C}}} = \mathrm{e}^{-[i\nu+\Gamma/2-\gamma/2]\tau_1}\mathrm{e}^{-[i\omega+\gamma/2]\tau_2}\sin\tilde{\Omega}\tau_{21}\Theta(\tau_1)\Theta(\tau_{21}). \qquad (4)$$

Here $\mathcal{C} = |2\eta_R\Omega/\tilde{\Omega}r_1r_2|^2$, $\tau_{21} = \tau_2 - \tau_1$, $\tilde{\Omega} = \sqrt{\Omega^2 - \gamma^2/4}$ is the effective Rabi frequency and γ is the decay rate between a and c and η_R is an overall (Raman) factor.

The spontaneous (Raman) decay rate in Eq. (4) is

$$\Gamma/2 = 2\pi|G_{k_0}|^2|\alpha_p|^2\mathcal{D}(\nu_{k_0}),$$

with $G_{k_0} = g_p g_{k_0}/\Delta$ being the usual Raman matrix element with coupling strengths g_p and g_{k_0}, and detuning Δ, see Fig. 1; α_p is the amplitude of the pump coherent field, $\mathcal{D}(\nu_{k_0})$ is the density of states and $k_0 = (\nu_p - \omega_{bc})/c$.

The photon-photon correlation function for *two* RED molecules can be obtained from Eq. (4) as

$$G^{(2)}_{\mathrm{RED}}(1,1';2,2') = |\psi(1,2) + \psi(1',2')|^2 =$$

$$\mathcal{C}\{\mathrm{e}^{-\Gamma\tau_1}\mathrm{e}^{-\gamma\tau_{21}}\sin^2\tilde{\Omega}\tau_{21} + \mathrm{e}^{-\Gamma\tau_1'}\mathrm{e}^{-\gamma\tau_{21}'}\sin^2\tilde{\Omega}\tau_{21}' +$$

$$\mathrm{e}^{-(\Gamma/2)(\tau_1+\tau_1')}\mathrm{e}^{-(\gamma/2)(\tau_{21}+\tau_{21}')}\sin\tilde{\Omega}\tau_{21}\sin\tilde{\Omega}\tau_{21}' \times$$
$$2\cos[\nu(\tau_1 - \tau_1') + \omega(\tau_2 - \tau_2')]\}, \qquad (5)$$

with $\tau_1' > 0, \tau_1 > 0, \tau_2 > \tau_1$ and $\tau_2' > \tau_1'$.

The essential difference between Eqs. (3) and (5) is the presence of the drive field dependent sine functions. Physically, this describes the finite time, governed by $\tilde{\Omega}$, to promote the molecule from b to a. This is the reason $G^{(2)}_{\mathrm{RED}}$ vanishes when $\tau_1 = \tau_2$. Mathematically,

the vanishing $G^{(2)}_{\rm RED}$ is the result of quantum interference between the two paths of Fig. 2.

Finally, we note that the spontaneous Raman decay rate can be written in the suggestive form $\Gamma/2 = \gamma_o(\Omega_p^2/\Delta^2)$, where the pump Rabi frequency is $\Omega_p = \alpha_p g_p$ and the radiation decay rate for $a' \to b$, is given by $\gamma_o \simeq 2\pi|g(\omega_{a'b})|^2\mathcal{D}(\omega_{a'b})$. Therefore, Γ is usually small compared to γ_o or γ, and we may neglect it in Eq. (5).

The cosine factor in Eq. (5) may be written as $\cos[(r_1 - r_1')n_1\nu/c + (r_2 - r_2')n_2\omega/c]$ where $n_1(n_2)$ is the index of refraction surrounding D1(D2). The retarded times τ_1 and τ_1' are $\tau_1 = t_1 - n_1 r_1/c$ and $\tau_1' = t_1 - n_1(r_1 + d\sin\theta)/c$ and likewise for τ_2 and τ_2'. Thus, $\tau_{21}' = \tau_{21} - (n_2 - n_1)(d\sin\theta)/c$ and since $\tilde{\Omega}d/c$ is very small compared to $\tilde{\Omega}\tau_{21}$ we may take $\tau_{21}' = \tau_{21}$ as it appears in the sine terms and the exponential decay factors. Equation (5) may then be written as

$$G^{(2)}_{\rm RED} = 4\mathcal{C}{\rm e}^{-\gamma\tau_{21}}\sin^2\tilde{\Omega}\tau_{21}\cos^2\frac{1}{2}[\kappa_\nu(r_1' - r_1) + \kappa_\omega(r_2' - r_2)] \quad (6a)$$

The differential path lengths are taken to be the same, *i.e.* $r_1' - r_1 = r_2' - r_2 = d\sin\theta$; and the cosine interference factor takes the form $\cos[(n_1\nu/c + n_2\omega/c)d\sin\theta]$. Recalling that $\tau_{21} = t_2 - t_1 - (n_2 r_2 - n_1 r_1)/c$ and since $r_2 = r_1$ by construction, we can write $G^{(2)}_{\rm RED}$ as

$$G^{(2)}_{\rm RED} = 4\mathcal{C}{\rm e}^{-\gamma\tau_{21}}\sin^2[\kappa_\Omega(r - D)]\cos^2\left[\frac{1}{2}(\kappa_\nu + \kappa_\omega)d\sin\theta\right] \quad (6b)$$

where $\kappa_\Omega = \tilde{\Omega}(n_1 - n_2)/c$. Here, we have taken $t_{21} \approx m\pi/\tilde{\Omega} + (n_2 - n_1)D/c$ such that $\tau_{21} > 0$. Equation (6b) can be expressed in terms of x the detector positions from the normal to the line joining the two marker molecules using $\sin\theta = x/\sqrt{D^2 + x^2}$. In the limit when $x/D << 1$,

$$G^{(2)}_{\rm RED}(x) \approx 4\mathcal{C}{\rm e}^{-\gamma\tau_{21}}\sin^2[\kappa_\Omega x^2/2D]\cos^2[(\kappa_\nu + \kappa_\omega)xd/2D] \quad (6c)$$

Equation (6b) allows us to determine d by measuring x_p the distance to the peak. For example, taking $G^{(2)}_{\rm RED}$ from (6c) with $\gamma = 0$ and using $\partial G^{(2)}_{\rm RED}/\partial x = 0$ we find

$$\tan(\kappa_\Omega x_p^2/2D)\tan((\kappa_\nu + \kappa_\omega)x_p d/2D) = 2\kappa_\Omega x_p/(\kappa_\nu + \kappa_\omega)d \quad (7)$$

which yields d for a given x_p. This is directly analogous to the case of Young's interference where we use $kdx_m/D \approx \pi$ to infer d by measuring the distance to the minimum x_m. There remains the question of which value of $\tilde{\Omega}$ to choose. It turns out that the sensitivity is enhanced by adjusting $\tilde{\Omega}$ so that the arguments of the $\sin^2$ and $\cos^2$ terms in (6b) are equal, this implies

$$G^{(2)}_{\rm RED}(\theta_p) = \mathcal{C}\mathrm{e}^{-\gamma\tau_{21}} \sin^2\left[(\kappa_\nu + \kappa_\omega)d\sin\theta_p\right]. \tag{8}$$

The first peak of Eq. (8) occurs when $2(\kappa_\nu + \kappa_\omega)d\sin\theta_p \cong \pi$, and if we take $\nu \approx \omega$ we have $2(n_1 + n_2)kd\sin\theta_p \cong \pi$. Thus we can now measure distances of order $d \approx \lambda/13$ using $n_1 = 1.9, n_2 = 2.1$ and $\sin\theta_p \approx 0.8$; this is summarized in Table 1. Sub-wavelength distances can be resolved with good sensitivity, as shown by Fig. 1b.

In summary, we underscore a few points.

The connection with photon-photon quantum erasure and subnatural spectroscopy : The quantum erasure scheme of [2] used a Raman (RED) configuration and sorted between fringes and antifringes via a cavity and shutter arrangement. The two-photon spectroscopy paper with Rathe [2] used the same detection scheme as in the present paper but with cascade (CED) radiation. Subensemble sorting with such a detection scheme is accomplished by tailoring the signal as seen by D2 relative to D1; see e.g. section 21.2.1 of ref. [10]. Furthermore in the experiment of [5] they say that: "[O]ne has to 'erase' the first-order interference by reinforcing an experimental condition : $\delta\theta > \lambda/b$, where $\delta\theta$ is the divergence of the light and b is the distance between the two slits.". It is also interesting to note that in the case of the three photon Raman scheme of Table 1e, we must end in level b_1 (register a D2 count) in order to assure that we have erased which way information.

The RED correlation function: Please note that the present calculation of $G^{(2)}(1,1';2,2')$ is based on the two-photon state $|\Psi\rangle$ of Fig. 2. The state $|\Psi\rangle$ is calculated via an extension of Weisskopf-Wigner theory [10]. The easier and more common approach to photon correlation calculations, involves focusing on the state of the molecule via a quantum regression analysis [11]. Finally we note that the null in $G^{(2)}_{\rm RED}(x)$ at $x = 0$ is essentially the same physics as photon antibunching.

The quantum interference microscope: First we note that the effective CED wavelength is $\sim 2\lambda_{\text{incident}}$ whereas for RED it is $\sim \lambda_{\text{incident}}$, thus yielding a factor of two resolution improvement for RED. Furthermore, the form of $G^{(2)}_{\text{RED}}$ (see Fig. 2) allows for further enhancement of resolution. Note also that when the indices n_2 and n_1 are equal we lose this enhanced resolution in the present scheme. In particular it may well be the case that the "signal" photons from A and B will propagate through vacuum, so that $n_1 = 1$ but $n_2 \neq 1$ in the half plane of the correlated photon; this is the case presented in Table 1. The net result is that it is possible to measure distances smaller than $\lambda/10$ via Raman photon pairs.

The best protocol for maximizing sensitivity is subtle. For example the difference in peak height between the red and black curves of Fig. 1b shows that the (properly normalized) value of $G^{(2)}(x_p)$ contains information about d. Such considerations will be discussed elsewhere. Likewise the application to lithography and other forms of microscopy will be the subject of future publications.

The author wishes to thank R. Austin, E. Fry, S. Harris, J. Kimble, K. Lehmann, M. Lukin, A. Muthukrishnan, R. Ooi, A. Patnaik, Y. Rostovtsev, A. Sokolov, W. Warren and S. Zubairy for stimulating and helpful discussions; and DARPA-QuIST, ONR, the Welch Foundation(Grant No. A-1261) and AFOSR(Rome) for support.

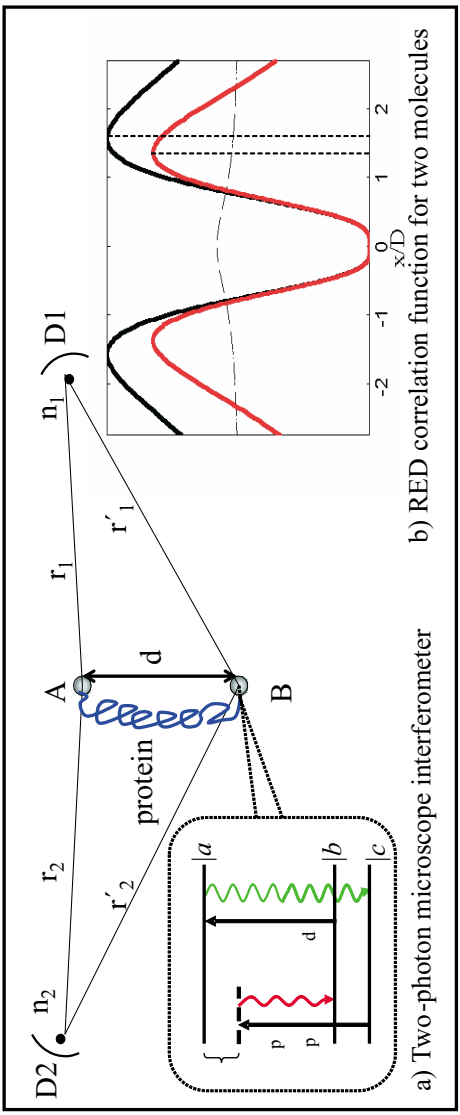

FIG. 1. a)Marker molecules or quantum dots at A and B generate correlated pairs of photons by a Raman quantum eraser process in which the scatterers are pumped by a laser (frequency ν_p) to a virtual level (dashed line) and spontaneously emit the first (Stokes) photon (ν). The molecule is then promoted from $b \rightarrow a$ by absorbing a drive laser photon (frequency ν_d) and spontaneously emits the second (anti-Stokes) photon (ω). The medium on the right (left) half plane has refractive index $n_1 = 1.9 (n_2 = 2.1)$. b) The correlation function for two RED molecules (A and B) is plotted from Eq. (6b) (solid lines), along with the single photon result (dashed line) for $d = d_o = \lambda/8$ (black line) and $d = 1.02 d_o$ (red line). Here, we take $\tilde{\Omega} = 10^9 s^{-1}$, D=1/3m and for simplicity, $\gamma = 0$. Note the strong dependence of $G^{(2)}_{\rm RED}$ on d (as indicated by the dotted lines to the separate peaks) whereas the single photon curves for d_o and $1.02 d_o$ are essentially the same, i.e. provide no microscopic resolution.

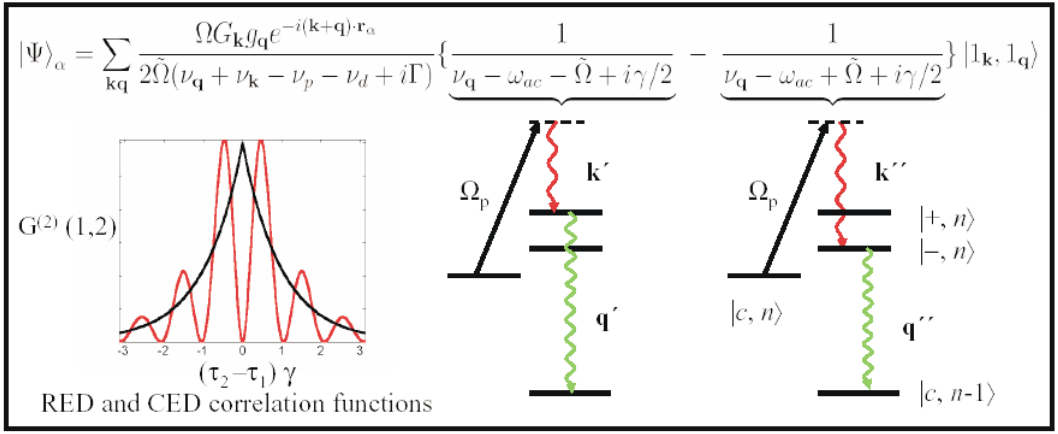

FIG. 2. The RED state for the molecule (at α=A or B) with spontaneously emitted, strongly correlated, photons having frequencies $\nu_{\mathbf{k}} \simeq \nu_p - \omega_{bc}$ and $\nu_{\mathbf{q}} \simeq \nu_d + \omega_{bc}$. In the figure $\nu_{\mathbf{k}}$ and $\nu_{\mathbf{q}}$ are depicted as red and green. This is artistic license, the color coding of ν_k and ν_q is used solely to guide the eye. Usually the frequency interval ω_{bc} is much less than ν_p or ν_d and so the frequencies ν_k and ν_q are approximately the same. The driving laser can be thought of as "dressing" the molecules resulting in the Autler-Townes splitting indicated. In order to make the physics clear, a photon number state $|n\rangle$ is assigned to the drive laser, although the actual state of the laser is a superposition of such number states. That is, the molecule-field system proceeds as $|c, n\rangle \rightarrow |\pm, n\rangle \rightarrow |c, n-1\rangle$. As indicated, there are two paths corresponding to $\mathbf{k}', \mathbf{q}'$ and $\mathbf{k}'', \mathbf{q}''$ pair emission, and they interfere destructively, leading to the zero in $G^{(2)}_{\rm RED}(1,2)$ when $\tau_2 = \tau_1$. This is shown in the (insert) plot of the photon-photon correlation function $G^{(2)}(r_1, t_1; r_2, t_2) = G^{(2)}_{\rm RED}(1,2)$ for one RED molecule (red), computed from Eq. (4) as a function of the difference in "retarded" times, see text. This is to be compared with that for CED (black).

References

[1] R. J. Glauber, Phys. Rev. **130**, 2529 (1963).

[2] M. Scully and K. Drühl, Phys. Rev. A **25**, 2208 (1982); M. Scully, ONR Workshop on Quantum Coherence 1993, and U. Rathe and M. Scully, Lett. Math. Phys. **34**, 297(1995). For a CED quantum eraser, see H. Huang and G. S. Agarwal, J. Mod. Opt. **42**, 465 (1995) and for a recent quantum eraser scheme which uses polarization for ensemble sorting, see P. Schwindt, P. Kwiat, and B. G. Englert, Phys. Rev. A 60, 4285 (1999).

[3] A. Boto, P. Kok, D. Abrams, S. Braunstein, C. Williams, and J. Dowling, Phys. Rev. Lett. **85**, 2733 (2000).

[4] For recent papers on quantum imaging see: M. D'Angelo, and Y. Shih, e-print quant-ph/0302146; A. Gatti, E. Brambilla, M. Bache, and L. Lugiato, Phys. Rev. A **70**, 013802 (2004); R. Bennink, S. Bentley, and R. Boyd, Phys. Rev. Lett. **89**, 113601 (2002); A. Abouraddy, B. Saleh, A. Sergienko, and M. Teich, Phys. Rev. Lett. **87**, 123602 (2001).

[5] M. D'Angelo, M. Chekhova, and Y. Shih, Phys. Rev. Lett. **87**, 013602 (2001).

[6] For an early quantum eraser experiment see: P. G. Kwiat, A. M. Steinberg, and R. Y. Chiao, Phys. Rev. A **45**, 7729 (1992); For a recent experiment along the lines of [2] see: Y. H. Kim, R. Yu, S. P. Kulik, Y. Shih, and M. O. Scully, Phys. Rev. Lett. **84**, 15 (2000); For applications of quantum eraser schemes to quantum information see: R. Garisto, and L. Hardy, Phys. Rev. A **60**, 827 (1999); G. Teklemariam, E. M. Fortunato, M. A. Pravia, T. F. Havel, and D. G. Cory, Phys. Rev. Lett. **86**, 5845 (2001).

[7] A. Kuzmich, W. Bowen, A. Boozer, A. Boca, C. Chou, L. M. Duan and H. Kimble, Nature **423**, 731(2003).

[8] C. van der Wal, M. Eisaman, A. Andre, R. Walsworth, D. Philips, A. Zibrov, M. Lukin, Science **301**, 196 (2003).

[9] S. Harris, Phys. Today **50**, 36 (1997).

[10] For analysis along these lines see M. Scully and S. Zubairy, "*Quantum Optics*", Cambridge Press (1997).

[11] A. Patnaik, G. Agarwal, R. Ooi, and M. Scully, to be published.